

## Chapter 5

# Structural Trends and the Influence of R-factors

### 5.1 Introduction

As mentioned in Chapter 4, a large number of studies of rare earth two dimensional silicides have now been published. This gives the opportunity to study the structural parameters (i.e. the RE–Si and Si–Si bond lengths) as a function of the rare earth. By doing so it may be possible to establish structural trends and similarities across the lanthanide series.

An examination of bulk rare earth silicides and the rare earth metals themselves reveals that one might well expect a trend to be apparent in some of the structural parameters of the 2D silicides. The Si–RE bond length in bulk rare earth silicides,  $RESi_{\sim 1.7}$ , has been shown to decrease as the mass of the rare earth increases [1]. Within the rare earth metals themselves there is a trend towards a decreasing atomic radius across the series [2]. These trends are summarised in Figure 5.1.

The trends mentioned above might suggest that a trend would be observed in the bond lengths of 2D RE silicides. On the other hand, the two dimensional rare earth silicides are known to be electronically similar [3-6]. As the Si<sub>1</sub>–Si<sub>2</sub> bond essentially just involves charge transfer from the RE, it might therefore be expected that this bond will remain fairly constant across the series. An examination of any trends it is possible to derive from published results and re-examination of data is presented below.

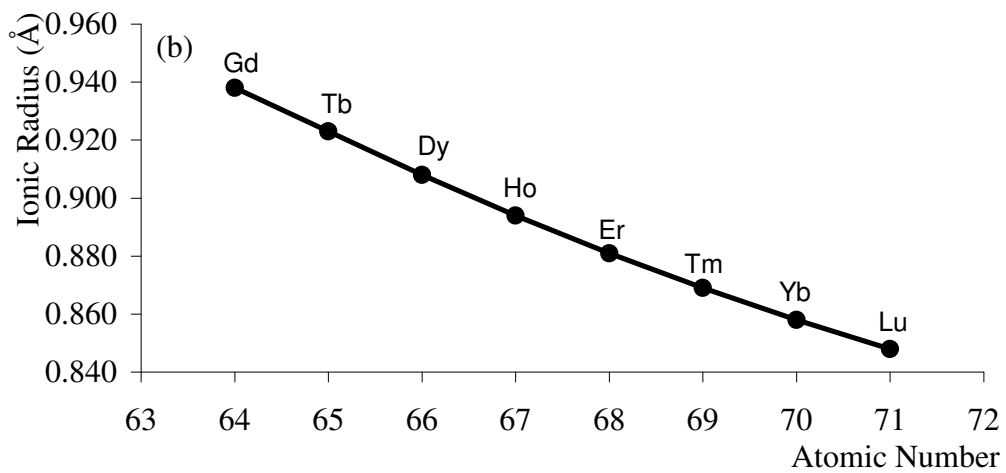
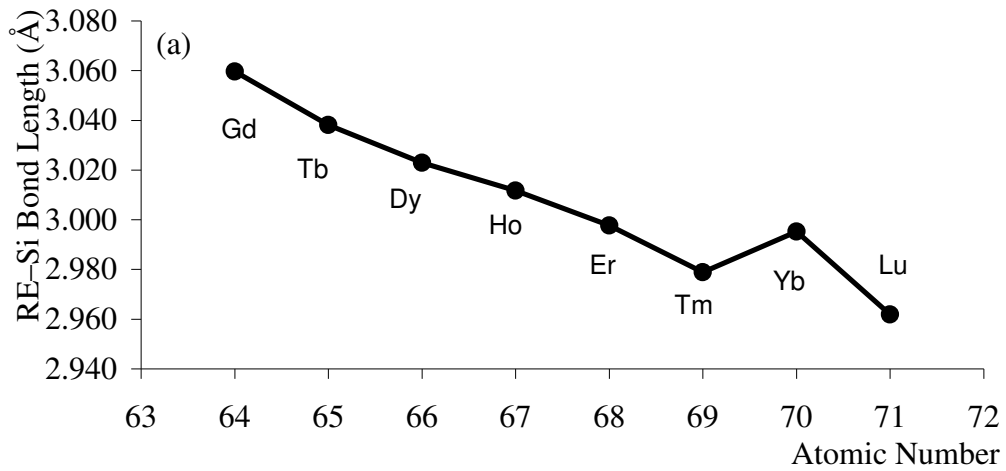


Figure 5.1: (a) RE-Si bond lengths in bulk rare earth silicides. (b) Ionic radii of rare earth metals. Both show a decreasing trend across the series.

## 5.2 A Possible Trend

Spence *et al.* [7] have previously mentioned the possibility of a trend in the structural parameters of 2D rare earth silicides. At the time there was only a limited set of data, crystallographic information being available for only the 2D silicides of Ho, Dy and Er. Table 5.1 collates all published crystallographic data for 2D RE silicides to date. As can be seen the data set available has been increased to include most trivalent rare earths.

As most of the studies have been by means of MEIS it is informative to directly compare the results from these studies. This also avoids any systematic variations due to the differences between techniques. Figure 5.2 and Figure 5.3 show a comparison of the experimental RE signals from MEIS double alignment scattering experiments for all the RE studies in which the author had access to the data, including the Tm 2D silicide described in the previous chapter. The scattering curves have been corrected for mechanical offset of the analyser and for the Rutherford scattering cross section as described

Rare Earth	Vertical Distance (Å)			Bond Length (Å)		Technique
	Si <sub>1</sub> -Si <sub>2</sub>	Si <sub>2</sub> -RE	Si <sub>1</sub> -RE	Si <sub>1</sub> -Si <sub>2</sub>	Si <sub>2</sub> -RE	
Y [8]	0.79 ± 0.04	1.85 ± 0.04	2.64 ± 0.06	2.35 ± 0.01	2.89 ± 0.03	LEED
Y [8]	0.74	1.77	2.51	2.34	2.84	DFT
Gd [9]	0.90 ± 0.02	1.86 ± 0.02	2.76 ± 0.02	2.39 ± 0.01	2.89 ± 0.01	MEIS
Dy [7]	0.85 ± 0.04	1.83 ± 0.03	2.68 ± 0.03	2.37 ± 0.02	2.87 ± 0.03	MEIS
Dy [10]	0.79 ± 0.03	1.90 ± 0.03	2.69 ± 0.04	2.35 ± 0.01	2.92 ± 0.02	LEED
Ho [11]	0.88 ± 0.04	1.80 ± 0.03	2.68 ± 0.03	2.39 ± 0.03	2.86 ± 0.03	MEIS
Ho [12]	0.82	1.88	2.70	2.36	2.91	LEED
Er [11]	0.92 ± 0.04	1.77 ± 0.03	2.69 ± 0.03	2.40 ± 0.03	2.83 ± 0.03	MEIS
Er [13]	0.82 ± 0.08	1.78 ± 0.08	2.60 ± 0.08	2.36 ± 0.03	2.84 ± 0.05	SXRD
Er [13]	0.80 ± 0.06	1.82 ± 0.06	2.62 ± 0.05	2.36 ± 0.02	2.87 ± 0.04	MEIS
Er [14]	0.90 ± 0.14	1.80 ± 0.10	2.70 ± 0.10	2.39 ± 0.05	2.86 ± 0.06	AED
Er [15]	0.78 ± 0.07	1.92 ± 0.05	2.70 ± 0.05	2.35 ± 0.02	2.93 ± 0.05	SEXAFS
Tm (This work)	0.86 ± 0.04	1.80 ± 0.03	2.66 ± 0.03	2.38 ± 0.02	2.86 ± 0.02	MEIS

Table 5.1: Published structural results for two-dimensional rare earth silicides. Refer to Figure 4.1 for atomic labels. Techniques other than MEIS show a longer Si<sub>2</sub>-RE bond length for a given rare earth.

Original in colour

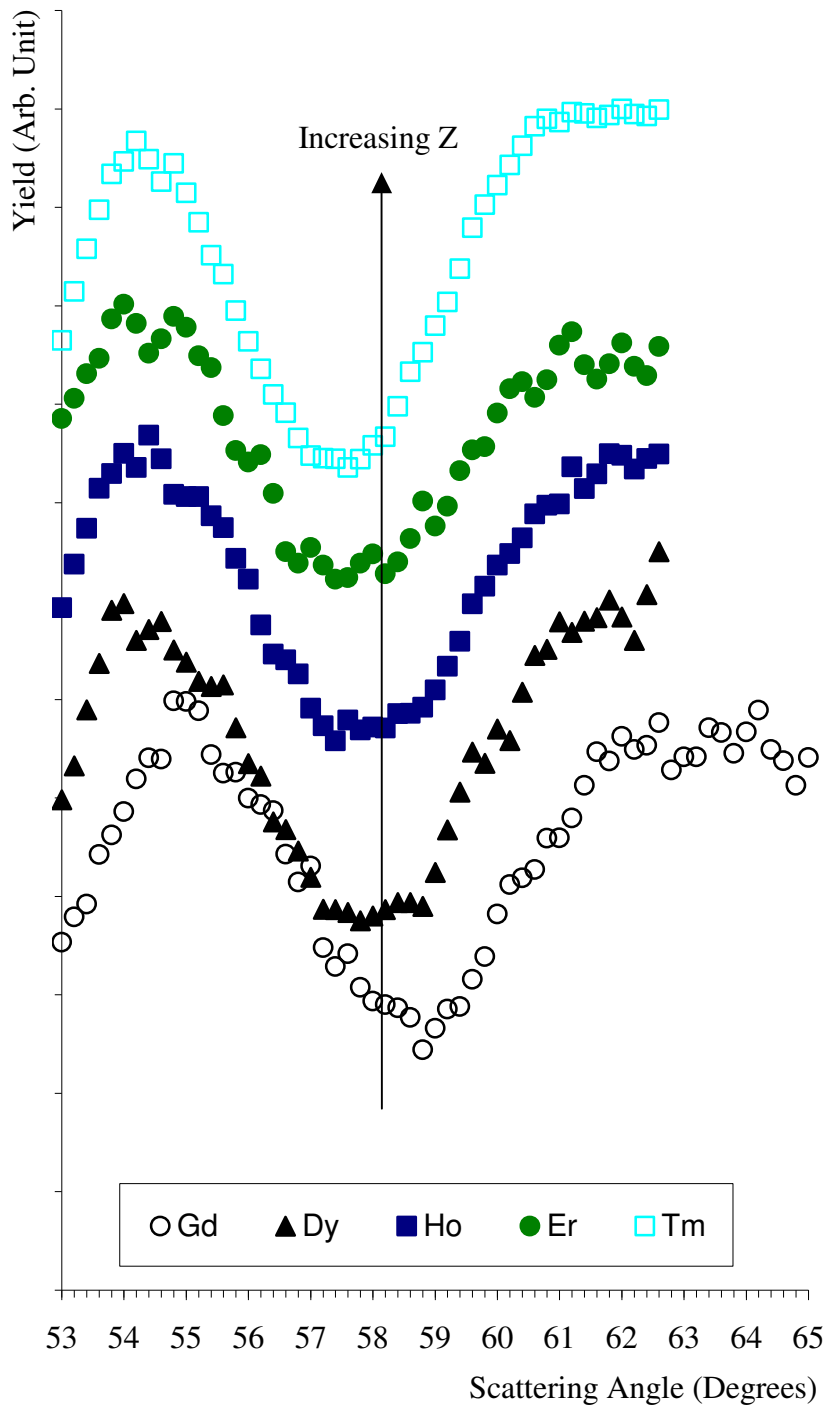


Figure 5.2: Comparison of experimental MEIS scattering curves for 2D rare earth silicides. This feature is due to the blocking of scattered ions by the  $\text{Si}_2$  atoms and directly reflects the  $\text{Si}_2$ -RE bond length (the blocking dip labelled  $\epsilon$  in the previous Chapter). Curves have been scaled to an arbitrary yield and then offset for clarity.

Original in colour

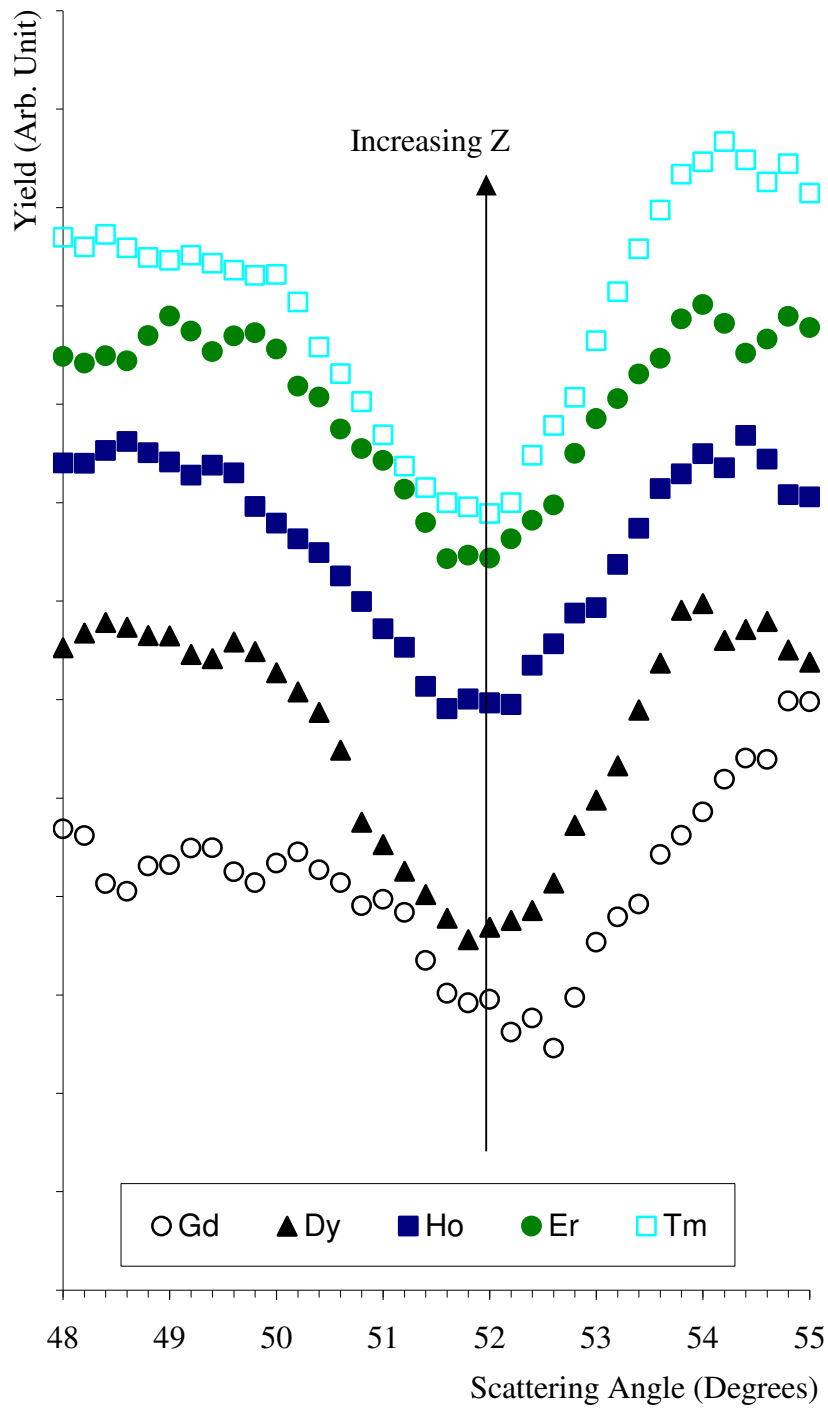


Figure 5.3: Comparison of experimental MEIS data for 2D rare earth silicides. The blocking dip shown is due to blocking of scattered ions by the  $Si_1$  atoms (the blocking dip labelled  $\delta$  in the previous Chapter). Curves have been scaled to a common arbitrary yield and then offset for clarity.

in Chapter 4. The curves have been scaled to a common yield, then each has been offset by a fixed amount for clarity. The blocking dip shown in Figure 5.2 is caused by scattered ions being blocked by the  $\text{Si}_2$  atoms (refer to Chapter 4 for atomic labels). There is a clear trend in the angular position of the blocking dip as the rare earth mass increases. This shift in blocking dip position represents a change in the  $\text{Si}_2$ -RE vertical distance and therefore a change in the bond length. The decreasing scattering angle with increasing atomic number corresponds to a decreasing bond length. This trend is partially evident in the published data (highlighted results in Table 5.1). The Tm result shows a discrepancy with the trend, which is discussed below. Figure 5.3 shows the blocking dip caused by scattered ions being blocked by the  $\text{Si}_1$  atoms. The position of this blocking feature is therefore indirectly related to the  $\text{Si}_1$ - $\text{Si}_2$  bond length.

### 5.3 The Possible Influence of the R-factor

As mentioned above, the results from the Tm data presented in the previous chapter do not fit with the trend seen in the structural parameters of other known 2D rare earth silicides. It may also be recalled from the previous chapter that the initial results for the Tm silicide were revised due to the R-factor analysis being overly influenced by one blocking feature. This caused the initially arrived at  $\text{Si}_2$ -Tm bond length to be revised upwards. If such an effect were present in the other 2D silicides then the Tm data may be found to match the trend in bond lengths.

Further indication that the previous MEIS results for 2D rare earth silicides may have been unduly influenced by the R-factor comes from a simple geometric consideration of the scattering angle at which the blocking dip occurs. A simple calculation based only on the scattering geometry leads to the  $\text{Si}_2$ -RE bond lengths given in Table 5.2. The published results described in Table 5.1 are shown for comparison. This calculation suggests that the published result for all but the  $\text{Si}_2$ -Tm bond length is actually too small (though the errors in the geometric calculation are of course quite large, there is a consistent indication of

Rare Earth	Calculated Si <sub>2</sub> -RE Bond Length (Å)	Published Bond Length (Å)
Gd	2.95 ± 0.04	2.89 ± 0.01 [9]
Dy	2.91 ± 0.04	2.87 ± 0.03 [7]
Ho	2.90 ± 0.04	2.86 ± 0.03 [11]
Er	2.90 ± 0.04	2.83 ± 0.03 [11]
Tm	2.87 ± 0.04	2.86 ± 0.02 (This work)

*Table 5.2: Bond lengths calculated from purely geometrical considerations (i.e. the measured angular position of the relevant blocking dip). Also shown for comparison are the published bond lengths.*

a longer Si<sub>2</sub>-RE bond length).

For 2D rare earth silicide systems where both MEIS and another technique have been used to quantitatively study the same system (the LEED studies of Dy [10] and Ho [12] and the various studies of Er [13-16]) the other techniques all indicate a longer Si<sub>2</sub>-RE bond length than that obtained from MEIS, again pointing towards the fact that the MEIS analysis is under estimating this value. Note that the Si<sub>1</sub>-Si<sub>2</sub> bond length is in general shorter in the other studies than that obtained from MEIS. Due to the nature of the MEIS analysis, which relates the vertical distance of the Si atoms relative to the RE, this is also consistent with the position of Si<sub>2</sub> being incorrectly determined. In effect the position of Si<sub>2</sub> should be higher than indicated by the MEIS studies, which would result in a lengthening of Si<sub>2</sub>-Re bond and shortening of Si<sub>1</sub>-Si<sub>2</sub> bond.

In the light of the above observations it seems that some further analysis of previously studied 2D rare earth silicides and of R-factors is necessary. The author has performed such an analysis, the results of which are now presented.

## 5.4 Re-examination of MEIS Structural Results

In Chapter 4 it was seen how a much better qualitative agreement between simulation and experiment could be achieved by excluding the lowest angle blocking dip in the  $[\bar{1} 00]/[\bar{1} 11]$  geometry from the R-factor analysis. In order to

Rare Earth	Revised $\chi$ -Squared		By Eye	
	Si <sub>1</sub> -Si <sub>2</sub> Bond Length (Å)	Si <sub>2</sub> -RE Bond Length (Å)	Si <sub>1</sub> -Si <sub>2</sub> Bond Length (Å)	Si <sub>2</sub> -RE Bond Length (Å)
Gd	2.36 ± 0.02	2.93 ± 0.02	2.36 ± 0.02	2.93 ± 0.03
Dy	2.36 ± 0.02	2.89 ± 0.02	2.36 ± 0.02	2.90 ± 0.03
Ho	2.37 ± 0.02	2.87 ± 0.02	2.36 ± 0.02	2.90 ± 0.03
Er	2.38 ± 0.02	2.86 ± 0.02	2.37 ± 0.02	2.88 ± 0.03
Tm	2.38 ± 0.02	2.86 ± 0.02	2.38 ± 0.02	2.86 ± 0.03

*Table 5.3: Revised structural parameters for 2D rare earth silicides and the corresponding subjective “by eye” fits. A general trend for a decrease in the Si<sub>2</sub>-RE bond length with increasing atomic number emerges.*

establish that this feature has skewed previous MEIS results to a too low Si<sub>2</sub>-RE bond lengths, the data to which the author has access have been reanalysed. A procedure similar to that used for the Tm silicide was used, comparing the existing simulations to the experimental data using a  $\chi^2$  R-factor excluding the lowest blocking dip from the calculation of the R-factor. The bond lengths thus obtained are indeed longer than those quoted in the literature. The newly revised structural parameters are given in Table 5.3. A subjective “by eye” fit (in which the angular position major blocking dips minima were subjectively fitted) was also performed, the results of which are also given in Table 5.3. Some confidence in the ability to fit such data by eye may be gained by considering not the bond lengths but the Si<sub>1</sub>-RE vertical distances. It is this quantity which is directly measured by the MEIS scattering curves, being given directly by the position of the  $\delta$  blocking dip. The vertical separation of Si<sub>1</sub>-RE for the original published results, the revised results and the by eye fits are shown in Table 5.4. This shows that the fitting of this lower angle blocking dip is not affected by the same issues as the fitting of the higher angle dip (see below for further discussion of these issues) and one may therefore “trust” the R-factor result, which shows almost no change between the published and revised results. The by eye fit is in very good agreement with these results, which demonstrates that it is possible to subjectively fit a blocking dip of this nature. The two blocking dips ( $\delta$  and  $\epsilon$ ) are quite similar in form and so it is reasonable to also employ a subjective fitting of

Si <sub>1</sub> –RE vertical separation (Å)			
Rare Earth	Published Result	Revised Result	By Eye Fit
Gd	2.76	2.74	2.74
Dy	2.68	2.67	2.66
Ho	2.68	2.67	2.66
Er	2.69	2.67	2.67
Tm	2.66	2.66	2.66

*Table 5.4: Vertical separations between the Si<sub>1</sub> and RE atoms as found in the original published results, from a revised study of the data and from fitting by eye. The by eye results show that it is possible to subjectively fit blocking dips of this form.*

the higher angle dip. It should be noted that it is once again the unusual independence of the blocking features in question which allows for such objective fitting.

The new bond lengths found by the revised study of the data and the by eye fitting are in better agreement with those derived from other techniques. A clear general trend is evident for the Si<sub>2</sub>–RE bond length to decrease as the mass of the rare earth increases. The Si<sub>1</sub>–Si<sub>2</sub> bond length remains approximately constant across the series.

## 5.5 Examining the R-Factor

### 5.5.1 *The Influence of the Low Angle Blocking Dip*

The influence of the lowest angle blocking dip within the  $[\bar{1} 00]/[\bar{1} 11]$  geometry in determining the best fit structural solution using a  $\chi^2$  R-factor comparison of simulation and experiment is readily demonstrable. Figure 5.4 shows the comparison between simulation and experiment for the structural solution determined using the R-factor (over the entire angular range) in the case of Tm 2D silicide (see Chapter 4 for a discussion of this system). Also shown on the graph is the contribution to the total R-factor from each angular point (0.2° apart). The lowest angle blocking dip can clearly be seen to provide the largest

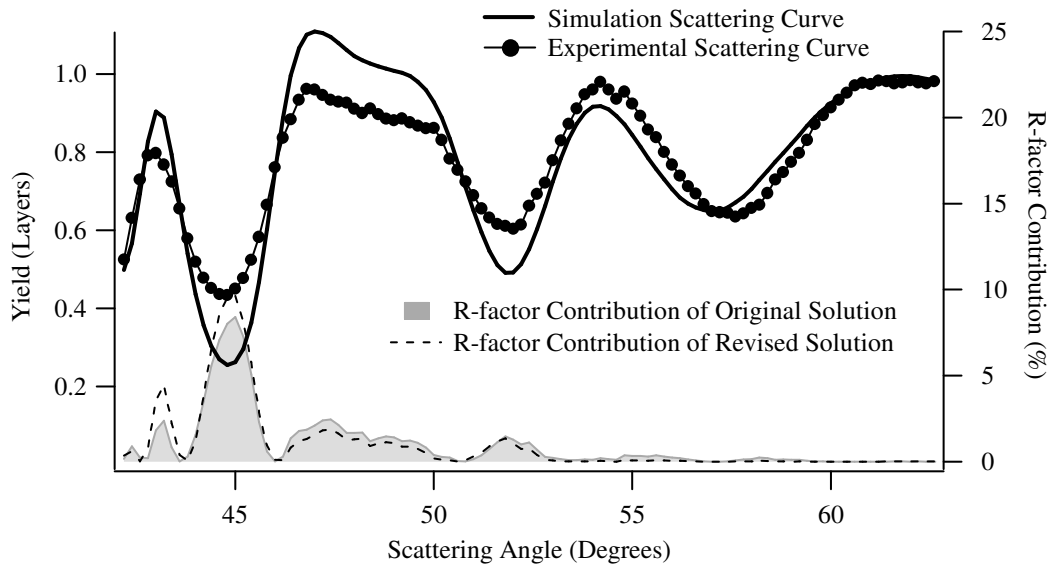


Figure 5.4: Contribution of each point to the total R-factor. Note the significance of the lowest angle dip. The dashed line shows similar contributions for the simulation of the final solution.

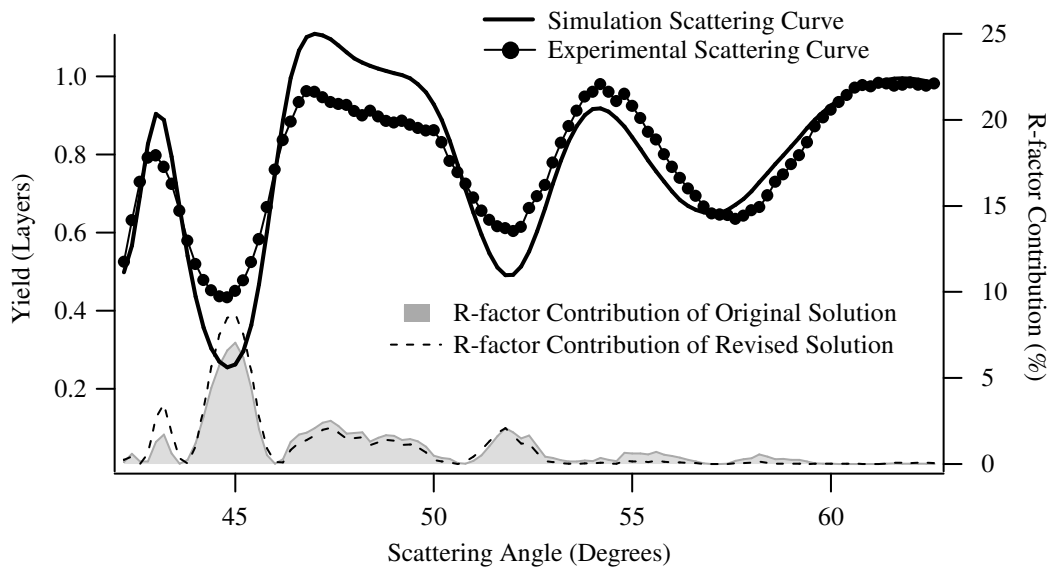


Figure 5.5: Contribution of each point to the total R-factor when the Rutherford scattering cross section is not taken into account. This eliminates the added weight given to lower angles due to the additional number of counts. The depth of the lowest angle dip is still the most important factor.

contribution. Furthermore, the dashed line shows the contribution to the R-factor from each point for the comparison to the simulation of the final solution. This clearly indicates that it is the difference in contribution due to the lowest angle dip which is having the greatest influence.

The  $\chi^2$  R-factor, i.e.

$$R_{\chi} = \frac{1}{N} \sum_{n=1}^N \frac{(Y_{\text{exp}} - Y_{\text{sim}})^2}{Y_{\text{exp}}} \quad (5.1)$$

gives most weight to points at which the yield is highest. When calculating the R-factor the fall off in counts due to the Rutherford scattering cross section is reintroduced. This results in the lower angles having a higher yield than higher angles and thus contributing proportionately more to the R-factor. While there is a good argument that this practice is indeed correct as the original data contained less counts at higher scattering angle and therefore must be less statistically significant at higher angles, it is an obvious exercise to recalculate the R-factor without this correction. This might be expected to reduce the significance of the lowest angle blocking dip and therefore improve the performance of the R-factor.

Such a comparison is shown in Figure 5.5. The structural solution chosen by the R-factor does not change, and the R-factor is still dominated by the lowest angle dip.

In fact the  $\chi^2$  R-factor is being influenced by the large difference in simulated and experimental yield around the lowest angle dip. This results in it discounting most of the structural information contained in the position and shape of all the other dipoles. Eliminating the lowest angle dip from the calculation of the R-factor produces contributions as shown in Figure 5.6.

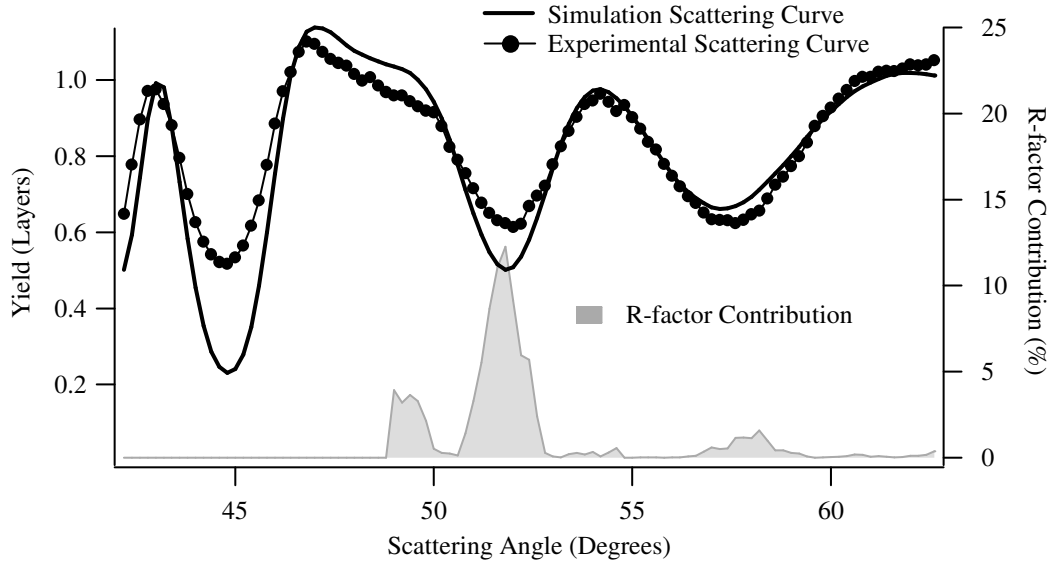


Figure 5.6: Contributions to the  $R$ -factor when discounting the lowest angle dip from the calculation of the  $R$ -factor. This produces a much better fit to the higher angle dips than that shown in Figure 5.4 and Figure 5.5.

### 5.5.2 Alternative $R$ -Factors

Numerous  $R$ -factors have in the past been applied to the comparison of theoretical and experimental scattering curves in MEIS. Noakes *et al.* [17] have previously compared several different  $R$ -factors in determining a structural solution to the Ni(100)c(2 × 2)-O system. They found that for that system at least any of the  $R$ -factors could be used to successfully identify a consistent structure. As well as  $R_\chi$  they examined

$$R_{IS} = \frac{100}{N} \left[ \sum_{i=1}^N \left( \frac{Y_{\text{exp}} - Y_{\text{sim}}}{Y_{\text{exp}}} \right)^2 \right]^{1/2}, \quad (5.2)$$

$$R_P = \frac{\sum_{i=1}^N (y_{\text{exp}} - y_{\text{sim}})^2}{\sum_{i=1}^N (y_{\text{exp}}^2 + y_{\text{sim}}^2)} \quad (5.3)$$

and

$$R_m = \frac{\sum_{i=1}^N (\chi_{\text{exp}} - \chi_{\text{sim}})^2}{\sum_{i=1}^N (\chi_{\text{exp}}^2 + \chi_{\text{sim}}^2)} \quad (5.4)$$

$R_{IS}$  is, like  $R_\chi$ , sensitive to the absolute yields of the simulated and experimental curves as well as the position of blocking features.  $R_{IS}$  and slight variants upon it have been used with some success in a number of MEIS studies [18-21].  $R_P$ , on the other hand, is the Pendry R-factor widely used in LEED [22]. In this R-factor,  $y$  is the logarithmic derivative of the intensities. Sensitivity to absolute yields is hence completely removed for well separated features and the R-factor is only sensitive to positions.

Finally  $R_m$  comes from the field of photoelectron diffraction. It is similar in form to Pendry's R-factor, with the term  $\chi$  being given by

$$\chi = (Y - Y_0) / Y_0 \quad (5.5)$$

$Y_0$  being a smooth spline which passes through the curve to be fitted.  $R_m$  thus has the advantage of being sensitive to both peak position and the absolute values of the intensity modulations but not to the intensities themselves.

These R-factors have been used to compare the experimental 2D rare earth silicide data to the Monte Carlo simulations. Two other R-factors have also been tested. The first of these is actually Pendry's R-factor but applied to data which has first been "flipped" (i.e. performing the conversion  $Y_{\text{flip}} = Y_{\text{max}} - Y$ ), hereafter  $R_{P\text{flip}}$ . This is more consistent with the type of data with which the R-factor is designed to deal, which is assumed to be a series of Lorentzian peaks. Indeed for some MEIS data this flipping has been seen to produce curves which are visually indistinguishable from those obtained from LEED  $I-V$ , though in the case of 2D rare earth silicides the effect is less dramatic.

The second R-factor attempts to produce an algorithm close to a naive “by eye” examination. The angular position of the minima within the experimental and simulated scattering curves are found and the R-factor taken to be

$$R_{\min} = \sum_{i=1}^M (\theta_{\text{sim}} - \theta_{\text{exp}})^2 \quad (5.6)$$

M being the number of minima found and  $\theta$  the angle at which the minimum occurs. This is somewhat similar to some R-factors which have been used in LEED, where the energy difference in peak positions was employed [23]. It suffers the same disadvantages, namely a disregard for intensity and ambiguities relating to the number of dips and which simulated dip matches which experimental dip. However, for a case such as the present, where the sequence of simulations produce similar intensities and number of dips and it is generally only the position of those dips which is changing, then it may be a useful tool in the determination of the correct structure.

### 5.5.3 Performance of the R-factors

The results of comparisons using each of these R-factors are summarised in Table 5.5. Some additional remarks should be noted, particularly in the case of the Pendry R-factors. One important parameter in the calculation of the Pendry R-factor is the imaginary part of the electron self energy,  $V_{oi}$ . This parameter is related to the width of the peak by  $\Delta E = 2 |V_{oi}|$ , where  $\Delta E$  is the half width half maximum (HWHM). In LEED  $|V_{oi}|$  is known to be around 4 eV. For application to MEIS it would seem sensible to choose a value equal to half the average width of a blocking dip. Given Equation 3.12 for the width of a blocking dip,

$$\psi = 4 \left( \frac{A}{Es} \right)^{1/2} \quad (5.7)$$

and taking a value for the distance between scattering, and blocking ion consistent with published structural parameters for rare earth silicides, one

Rare Earth	Bond	$R_\gamma$	$R_\gamma$ Refined	$R_{IS}$	$R_m$	$R_P (V_{oi}=1.5)$	$R_P (V_{oi}=7.5)$	$R_{Pflip}$	$R_{min}$	“By Eye”
Gd	Si <sub>1</sub> -Si <sub>2</sub> (Å)	2.39 ± 0.01	2.36 ± 0.02	2.40 ± 0.02	2.40 ± 0.02	2.39 ± 0.02	2.37 ± 0.02	2.36 ± 0.02	2.36 ± 0.02	2.36 ± 0.02
	Si <sub>2</sub> -RE (Å)	2.89 ± 0.01	2.93 ± 0.02	2.89 ± 0.03	2.91 ± 0.03	2.95 ± 0.03	2.92 ± 0.03	2.92 ± 0.03	2.93 ± 0.03	2.93 ± 0.03
Dy	Si <sub>1</sub> -Si <sub>2</sub> (Å)	2.37 ± 0.02	2.36 ± 0.02	2.39 ± 0.02	2.40 ± 0.02	2.37 ± 0.02	2.36 ± 0.02	2.35 ± 0.02	2.37 ± 0.02	2.36 ± 0.02
	Si <sub>2</sub> -RE (Å)	2.87 ± 0.03	2.89 ± 0.02	2.86 ± 0.03	2.84 ± 0.03	2.90 ± 0.03	2.90 ± 0.03	2.90 ± 0.03	2.89 ± 0.03	2.90 ± 0.03
Ho	Si <sub>1</sub> -Si <sub>2</sub> (Å)	2.39 ± 0.03	2.37 ± 0.02	2.39 ± 0.02	2.37 ± 0.02	2.35 ± 0.02	2.35 ± 0.02	2.35 ± 0.02	2.36 ± 0.02	2.36 ± 0.02
	Si <sub>2</sub> -RE (Å)	2.86 ± 0.03	2.87 ± 0.02	2.85 ± 0.03	2.86 ± 0.03	2.88 ± 0.03	2.89 ± 0.03	2.89 ± 0.03	2.88 ± 0.03	2.90 ± 0.03
Er	Si <sub>1</sub> -Si <sub>2</sub> (Å)	2.40 ± 0.03	2.38 ± 0.02	2.40 ± 0.02	2.40 ± 0.02	2.39 ± 0.02	2.38 ± 0.02	2.35 ± 0.02	2.37 ± 0.02	2.37 ± 0.02
	Si <sub>2</sub> -RE (Å)	2.83 ± 0.03	2.86 ± 0.02	2.84 ± 0.03	2.84 ± 0.03	2.85 ± 0.03	2.86 ± 0.03	2.89 ± 0.03	2.87 ± 0.03	2.88 ± 0.03
Tm	Si <sub>1</sub> -Si <sub>2</sub> (Å)	2.39 ± 0.02	2.38 ± 0.02	2.40 ± 0.02	2.39 ± 0.02	2.37 ± 0.02	2.38 ± 0.02	2.37 ± 0.02	2.37 ± 0.02	2.38 ± 0.02
	Si <sub>2</sub> -RE (Å)	2.84 ± 0.02	2.86 ± 0.02	2.84 ± 0.03	2.84 ± 0.03	2.86 ± 0.03	2.86 ± 0.03	2.86 ± 0.03	2.86 ± 0.03	2.86 ± 0.03

Table 5.5: Comparison of the best fit models derived from comparing simulated and experimental blocking curves using a variety of R-factors. Also shown are the best subjective visual fits (“By Eye”). A trend in the Si<sub>2</sub>-RE bond length is apparent in the results from a number of comparison methods; notably the “by eye” comparison,  $R_{min}$ ,  $R_{Pflip}$  and  $R_\gamma$ -refined.

obtains a width of around  $3\frac{1}{2}$ – $6^\circ$ . There will be some broadening due to thermal effects, so it seems reasonable to accept a value of around  $2$ – $3^\circ$  for the HWHM (a value consistent with the scattering curves from the rare earth silicides). This gives a value of  $V_{oi}$  of  $1$ – $1\frac{1}{2}^\circ$ .

Having performed the above analysis it was found that the Pendry R-factor failed to consistently arrive at a convincing solution for the best fit simulation. Whilst on some occasions the solution would appear to be a good fit, on others a visual inspection immediately revealed that the suggested solution was clearly incorrect. It was discovered, by a trial and error means, that the performance of the Pendry R-factor could be improved by using a value for  $V_{oi}$  of  $7\frac{1}{2}^\circ$ . This would imply a HWHM of the blocking dips of around  $15^\circ$ , which can clearly be seen not to be the case by looking at such a blocking dip. Indeed  $15^\circ$  is over half the typical angular range for a scattering curve (the MEIS analyser accepting ions over a scattering window of  $27^\circ$ ). There seems to be no physical basis for this choice of  $V_{oi}$  and due to the empirical nature of its determination it is possible that further optimisation is achievable. It is likely that the requirement for such a high value of  $V_{oi}$  is due to the R-factor attempting to fit Lorentzian peaks to a data set which consists of relatively flat regions and large *dips*. It is also possible that an entirely different value of  $V_{oi}$  would be required for use with scattering curves from a different structure. This does not make for a satisfactory R-factor.

The above failings in the Pendry R-factor led to the development of  $R_{Pflip}$ , in which the scattering curves are first inverted before calculation of the R-factor. This, at least qualitatively, produces a curve more reminiscent of the LEED  $I$ – $V$  curves with which the Pendry R-factor has proven a success (see Figure 5.7). The initial estimate for the value of  $V_{oi}$  was again used. The “flipped” version of the Pendry R-factor (this is a somewhat misleading term—the R-factor remains the same but the data from which it is calculated has been “inverted”) selected a simulation which was a much better match to the experimental data than its predecessor did. This R-factor did still require some smoothing of the

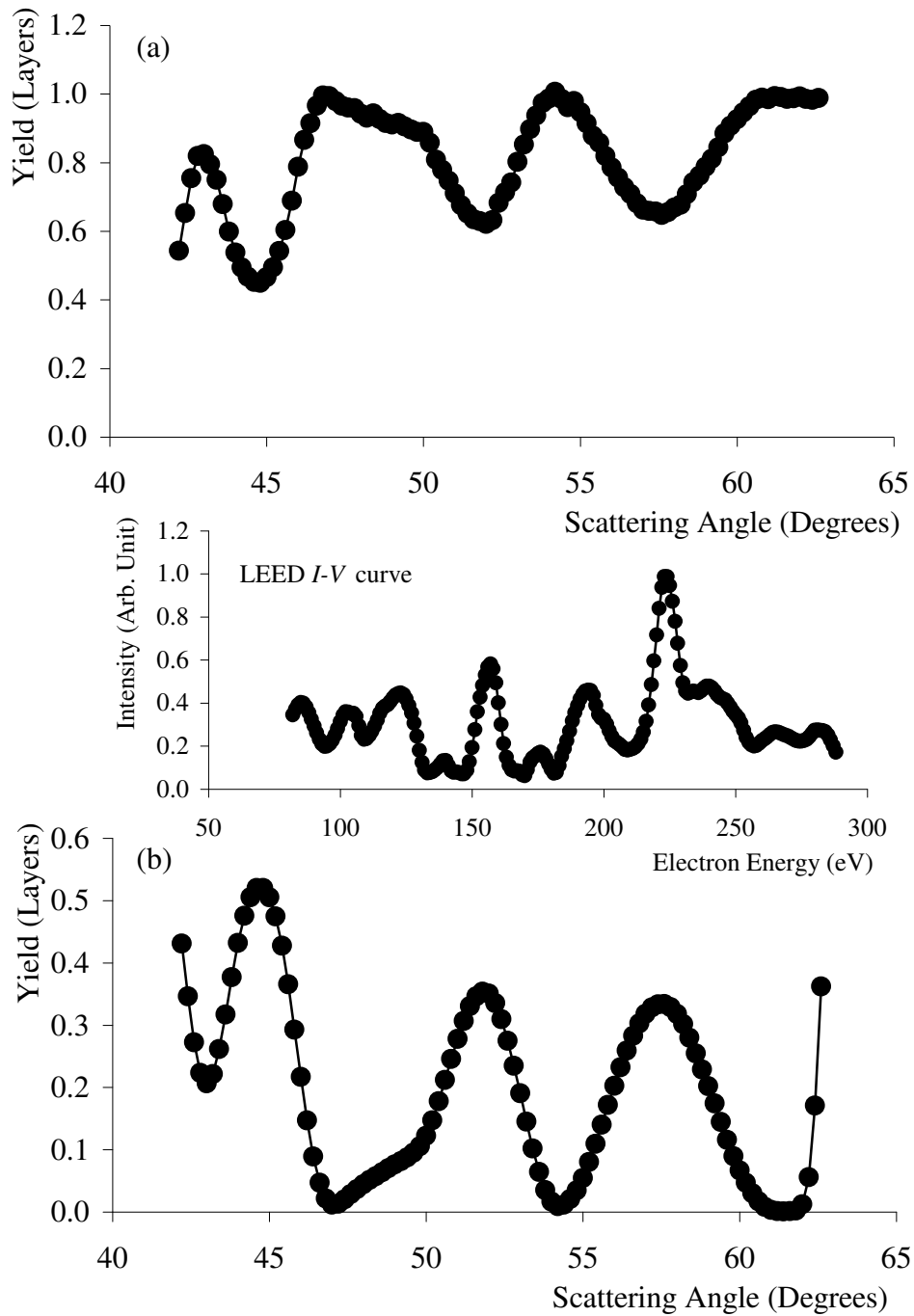


Figure 5.7: Comparison of (a) the original Tm silicide MEIS scattering curve and (b) the “flipped” version. The inset shows a typical LEED I–V curve [10]. The Pendry R-factor was originally designed to deal with peaks rather than dips. The flipped data may be considered qualitatively more like the LEED data for which the Pendry R-factor is standard.

experimental data in order to reduce the effects of noise but this had been a requirement for the original  $R_P$  with  $V_{oi} = 7.5$  as well.

The R-factors  $R_{IS}$  and  $R_m$  performed poorly. In the case of  $R_{IS}$  this is probably due to the same issues observed for  $R_\chi$ . The performance of  $R_m$  may have been influenced by the fit of the smooth spline to the scattering curves. The solutions were as poor a match as those found by the original  $R_\chi$  and on occasion worse.  $R_{min}$  appears to reproduce the process of selecting the best fit model by eye well. However, it seems likely that this R-factor is not very robust when confronted with more complex data sets. It may prove useful in some cases, especially with blocking features which have a single origin.

#### 5.5.4 *Errors in the Results*

The errors quoted in Table 5.5 deserve some mention. Those for  $\chi^2$  R-factors are calculated from Equation 4.2 and are comparable with those in the literature. The errors quoted for the “by eye” fits were estimated as for the case of Tm silicide in the previous chapter, i. e. they are themselves quite subjective but err on the side of caution—it was felt that each parameter could be fitted to within two or three steps of the simulations.

In the case of the Pendry R-factor it is usual in LEED to estimate the error using the variance in the minimum value of the R-factor [22]

$$\text{var}(R_{\min}) = R_{\min} \sqrt{2/N} \quad (5.8)$$

(strictly this is a standard deviation but it is common to maintain Pendry’s original nomenclature).

Here,  $N$  is the number of pieces of independent information contained within the data. In terms of LEED this is easily given by the number of well separated peaks which could be present. For the Lorentzian peaks involved, the full width half maximum is given by  $2 V_{oi}$ , so well separated peaks occupy an energy width of 4

$V_{oi}$  and  $N$  is given by

$$N = E / (4 V_{oi}) \quad (5.9)$$

where  $E$  is the total energy range over which data is taken.

Relating the above to the case of the 2D silicides, Equation 5.9 would imply that for a single geometry (angular range  $27^\circ$ )  $N = 4.5$  for  $V_{oi} = 1.5$ . Over the two geometries available this would then give  $N = 9$ .

Another obvious estimate of  $N$ , in the case of MEIS, is the number of blocking features actually present (neglecting the fact that the features are not necessarily independent). For the 2D silicides this would give  $N = 5$  for the two geometries available. This value is probably an underestimate as it only counts large blocking features, neglecting more subtle effects, and fails to account for the fact that the absence of a blocking feature may also convey structural information.

From the above arguments it would seem that a value of  $N$  in the region of 5–10 is not unreasonable. However, calculations using Equation 5.8 resulted in unrealistically large errors for each structural parameter. This may be related to the fact that in LEED a very small change in the structural model results in large changes in the I–V curves, whereas in MEIS—and especially in the case of 2D silicides—small structural parameter changes have only a small effect on one or two blocking features, which maintain their overall character. The R-factor curve around the minimum R-factor may therefore be expected to be steeper in LEED than MEIS.

The errors quoted for Pendry R-factors are hence not based on a quantitative calculation but rather estimated assuming that the selected model is correct within two steps for each parameter (i.e. the error in parameter  $a_j$  was taken to be  $2\delta z_j$  where  $\delta z_j$  is the change in  $a_j$  between models of the multicalc). It also seems reasonable to assume that the maximum error in using an R-factor guided fit is no greater than that which can be achieved by fitting by eye.

Errors quoted for other R-factors have been estimated in an identical way as for the Pendry R-factors. It is an obvious advantage of the  $\chi^2$  R-factor that it offers a quantitative way in which to calculate the error in each parameter. It is felt that this is probably an over estimate of the true error in the results. Ideally the R-factor should distinguish just one structural model as the solution, implying an error of around half the parameter step size. Whilst it is not anticipated that the precision would necessarily be this good in the present case, a more realistic error would probably be something slightly less than those quoted, more reminiscent of those achieved using the revised  $\chi^2$  R-factor, i.e. around  $\pm 0.02$  Å at worst—at least for those R-factors which appear to perform consistently.

More importantly, a trend in the Si<sub>2</sub>–RE bond length does emerge. Although such a trend is seemingly masked by the errors associated with the bond lengths, the weight of evidence points towards it. The trend consistently emerges whichever R-factor is used in the comparison. Further, visually comparing the data to the simulations, a method shown above to be at least partly reliable, and which in this case has possibly the largest over estimate of error, also shows a trend in the bond length. Perhaps the most compelling argument is the obvious visual shift in the position of the blocking dip as demonstrated in Figure 5.2 (and reflected in the geometrical calculations summarised in Table 5.2). Whilst the absolute value of the bond length retains some uncertainty, the author feels justified in a confidence that the bond length does decrease with increasing RE atomic number.

#### 5.5.5 *Conclusion*

It has been shown that the selection of the best fit structural model based on an R-factor comparison of simulated and experimental blocking curves is, in the case of 2D rare earth silicides, problematic. Although the systems under consideration represent a special, and perhaps unusual case, these difficulties emphasise the importance of vigilance from the experimenter when examining data. Various other R-factors and workarounds have been tried. In the case of the Pendry R-factor improvements have been found by adjusting the data to better

resemble the LEED data that R-factor was designed to work with—this R-factor then gives the best general performance. While no completely satisfactory solution has been found, a combination of R-factors can give some confidence to the result.

## 5.6 Conclusion

A possible trend in the structural parameters of 2D rare earth silicides has been identified. Problems with the use of a  $\chi^2$  R-factor have been seen, which may have affected published results in the past. A variety of other R-factors have been applied to the experimental–simulation comparison, with varying degrees of success. The 2D rare earth silicides result in particularly peculiar MEIS scattering curves, in that the curves exhibit few, well defined blocking dips. This simplicity is thanks to the straight forward scattering and blocking geometries caused by the presence of only a single rare earth layer and the ability to isolate the scattering from this layer due to the mass separation. It might be expected that where the scattering data is more complex, as is the case in most systems, the problems associated with comparisons to model structures for the 2D silicides will not be so apparent. However, it is due to this simple, low number of blocking features that it is also possible to rapidly make a subjective assessment of fit. The R-factors which have been found to perform consistently, including adjustment of the range over which  $R_\chi$  is calculated, support the conclusion that previous studies have underestimated the length of the  $\text{Si}_2$ –RE bond whilst overestimating the  $\text{Si}_1$ – $\text{Si}_2$  bond length (i.e. they have placed the z-position of  $\text{Si}_2$  too “low”). This is consistent with results from other techniques such as LEED.

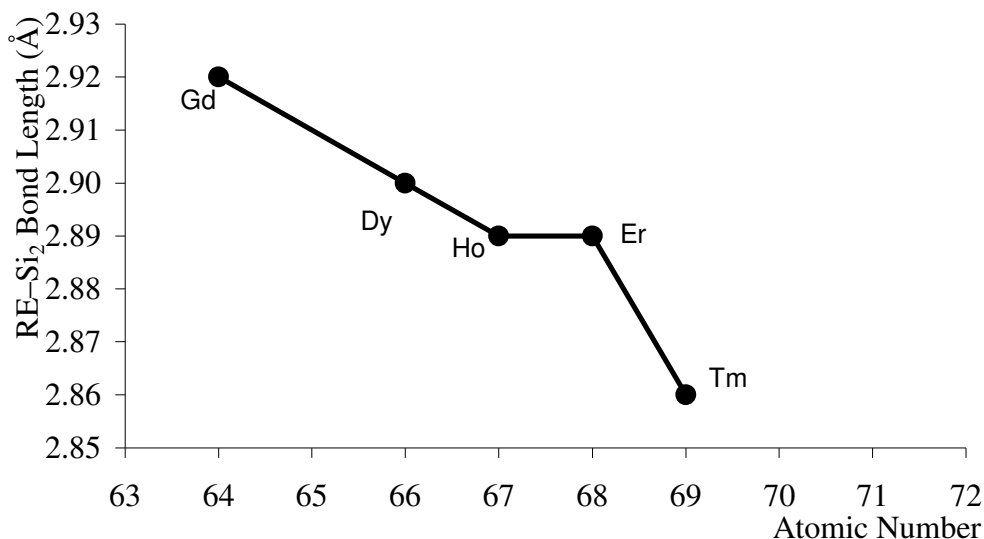


*Figure 5.8: The structural trend in the Si<sub>2</sub>–RE bond length across the rare earth series. This plot is derived from the structural model determined using  $R_{Pflip}$ . Other methods of determining the best fit model show a similar trend.*

A trend has emerged for the Si<sub>2</sub>–RE bond length to decrease as the mass of the rare earth metal in the silicide increases. This is illustrated in Figure 5.8 where the Si<sub>2</sub>–RE bond length, as determined using  $R_{Pflip}$ , is plotted as a function of the RE atomic number. This trend is actually apparent in a comparison of the experimental blocking curves from each silicide as demonstrated in Figure 5.2. The trend matches that known for the Si–RE bond length in the bulk silicide and reflects the decreasing ionic radii of the rare earths. The Si<sub>1</sub>–Si<sub>2</sub> bond length remains approximately constant across the series. It is hoped that identification of such a trend may be of some use in future work to build more complex systems based on 2D rare earth silicides.

## References

1. J. A. Knapp and S. T. Picraux, *Appl. Phys. Lett.* **48** 466 (1986)
2. S. D. Barrett, *Surf. Sci. Rep.* **14** 271 (1992)
3. S. Vandré, T. Kalka, C. Preinesberger and M. Dähne-Prietsch, *Phys. Rev. Lett.* **82** 1927 (1999)
4. S. Vandré, T. Kalka, C. Preinesberger and M. Dähne-Prietsch, *J. Vac. Sci. Technol. B* **17** 1682 (1999)
5. L. Stauffer, A. Mharchi, C. Pirri, P. Wetzel, D. Bolmont, G. Gewinner and C. Minot, *Phys. Rev. B* **47** 10555 (1993)
6. C. Rogero, C. Koitzsch, M. E. González, P. Aebi, J. Cerdá and J. A. Martín-Gago, *Phys. Rev. B* **69** 045312 (2004)
7. D. J. Spence, T. C. Q. Noakes, P. Bailey and S. P. Tear, *Surf. Sci.* **512** 61 (2002)
8. C. Rogero, C. Polop, L. Magaud, J. L. Sacedón, P. L. de Andrés and J. A. Martín-Gago, *Phys. Rev. B* **66** 235421 (2002)
9. D. J. Spence, S. P. Tear, P. Bailey and T. C. Q. Noakes, *Private Communication*
10. C. Bonet, D. J. Spence and S. P. Tear, *Surf. Sci.* **504** 183 (2002)
11. D. J. Spence, S. P. Tear, T. C. Q. Noakes and P. Bailey, *Phys. Rev. B* **61** 5707 (2000)

12. H. Kitayama, S. P. Tear, D. J. Spence and T. Urano, *Surf. Sci.* **482-485** 1481 (2001)
13. M. Lohmeier, W. J. Huisman, G. ter Horst, P. M. Zagwijn, E. Vlieg, C. L. Nicklin and T. S. Turner, *Phys. Rev. B* **54** 2004 (1996)
14. P. Wetzel, C. Pirri, P. Paki, D. Bolmont and G. Gewinner, *Phys. Rev. B* **47** 3677 (1993)
15. M. H. Tuilier, P. Wetzel, C. Pirri, D. Bolmont and G. Gewinner, *Phys. Rev. B* **50** 2333 (1994)
16. M. Lohmeier, W. J. Huisman, E. Vlieg, A. Nishiyama, C. L. Nicklin and T. S. Turner, *Surf. Sci.* **345** 247 (1996)
17. T. C. Q. Noakes, P. Bailey and D. P. Woodruff, *Nucl. Instrum. Meth. B* **136-138** 1125 (1998)
18. B. W. Busche and T. Gustafsson, *Phys. Rev. B* **61** 16097 (2000)
19. M. Chester and T. Gustafsson, *Surf. Sci.* **256** 135 (1991)
20. M. Copel, T. Gustafsson, W. R. Graham and S. M. Yalisove, *Phys. Rev. B* **33** 8110 (1986)
21. P. Fenter and T. Gustafsson, *Phys. Rev. B* **38** 10197 (1988)
22. J. B. Pendry, *J. Phys. C.: Solid State Phys.* **13** 937 (1980)
23. E. Zanazzi and F. Jona, *Surf. Sci.* **62** 61 (1977)